ISSN: 2414-1895 DOI: 10.6919/ICJE.202603_12(3).0047

Real-Time Acquisition Circuit for Irregular Flexible Pressure Sensor Arrays

Hao Dong, Haoran Yin, Xinrui Niu, Xiaofen Lin, and Zhengfa Hu

School of Physics and Optoelectronic Engineering, Guangdong University of Technology, Guangzhou 510006, China

Abstract

Irregular flexible pressure sensor arrays face critical bottlenecks of poor layout adaptability, low scanning efficiency, and high implementation cost in dynamic pressure monitoring. To address these challenges, this paper proposes a low-cost, high-real-time data acquisition system based on STM32microcontroller.For hardware, a configurable row-column addressing circuit withCD4052/CD4051analog multiplexers is designed to match compact irregular arrays, enabling0~5000g wide-range pressure sensing. For algorithm, a novel"1+4"fast scanning strategy is developed to optimize dynamic pressure detection, delivering51%higher efficiency than traditional full-traversal scanning. A Qt multi-threaded host computer is built for10Hz real-time heatmap visualization. Experimental results demonstrate that the system achieves±0.5N measurement accuracy and ≤50ms end-to-end latency under72MHz clock and 12-bit ADC configuration. This work fills the technical gap in low-cost real-time monitoring for irregular flexible arrays, and provides a reliable solution for smart medical mattresses and industrial robotic tactile perception.

Keywords

Irregular Flexible Sensor Array; Fast Scanning Algorithm; Microcontroller; Host Computer Serial Communication.

1. Introduction

Flexible array sensors have irreplaceable technical value in fields such as medical health (body pressure monitoring and physiological signal tracking)[1], industrial manufacturing (precision assembly pressure detection)[2,3], and robotics (skin-like tactile perception)[4], owing to their superior surface conformability and distributed sensing capability. However, existing sensing systems still face multiple bottlenecks in adaptability, cost, efficiency, and accuracy.

Most existing studies focus on regular square array designs. In practical applications, however, irregular layouts (e.g.,4×8) are more practical due to constraints of installation space and the shape of measured objects; regular arrays are prone to monitoring blind spots when attached to curved surfaces. For existing solutions targeting irregular arrays, FPGA-based custom driving schemes suffer from high cost and high power consumption, making them unsuitable for portable devices, while microcontroller-based full-traversal schemes have long scanning time, low efficiency, and insufficient accuracy.

To solve the above problems, this study develops a 4×8 irregular flexible array sensor system based on STM32. At the hardware level, a low-cost solution with domestic CD4052/CD4051 analog multiplexers and a 51kΩ calibration resistor is adopted to adapt to the compact layout of the irregular array. At the algorithm level, an innovative "1+4" fast scanning strategy combined with Kalman filtering[5] is proposed to shorten scanning time and reduce the miss detection rate. A linear

ISSN: 2414-1895 DOI: 10.6919/ICJE.202603_12(3).0047

conductance-pressure model (G=kP+b) and multi-sensor fusion are established to compensate for the measurement error of the irregular array. This work provides a low-cost, high-efficiency, and high-precision monitoring solution with irregular arrays for intelligent medical care[6], industrial inspection, and other scenarios.

2. Overall System Architecture

The proposed system adopts a hardware-software collaborative architecture, as shown in Fig. 1. The STM32F103C8T6 is used as the main control chip to drive CD4052/CD4051 analog multiplexers for time-division row-column scanning of the 4×8 flexible array. A voltage divider circuit built with a 51kΩ calibration resistor and a low-noise LDO is designed to suppress power supply interference[7] and ensure accurate acquisition of dynamic voltage signals ranging from 0.73~2.75V by the 12-bit ADC module.

At the software level, the embedded algorithm adopts the "1+4" fast scanning strategy and Kalman filter prediction, reducing the single-frame scanning time from 325ms to 145ms with a 55% efficiency improvement. The host computer is developed based on the PyQt6 multi-threaded architecture to realize asynchronous data reception and dynamic heatmap rendering. A custom four-segment color scale (white→green→yellow→red) is mapped via the seaborn library for dynamic visualization of pressure distribution.

In the collaborative workflow, the STM32 calculates the pressure value in real time (P=1000·(1/R−0.0023)) and transmits the data through a compact frame protocol (32 bytes/frame, 115200bps) with CRC-16 checksum. The host computer reconstructs the 4×8 pressure matrix after data parsing and triggers real-time visualization. This architecture realizes high-precision and low-latency pressure monitoring under the embedded resource constraints of STM32, providing a reliable solution for medical[8] and industrial scenarios.

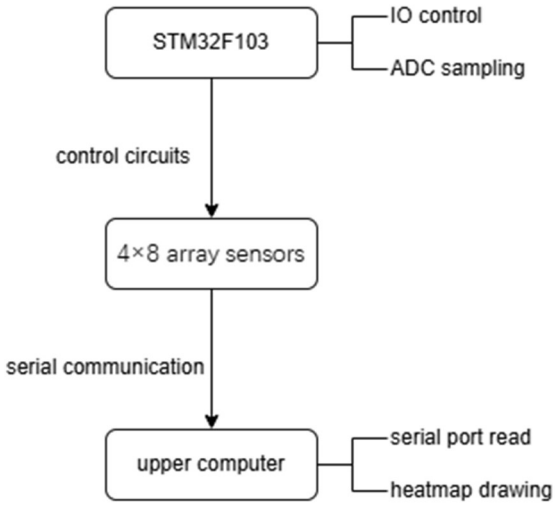

Fig. 1 System structure flow diagram

3. Core Hardware Design and Pressure Sensing Modeling

3.1 Key Hardware Design

To achieve low-power and low-cost driving of the 4×8 flexible array, the system adopts a hardware scheme of "STM32F103C8T6+CD4052/CD4051 analog multiplexers + 51kΩ calibration resistor". The core design is detailed as follows.

Main Control Chip and Addressing Circuit:

The STM32F103C8T6 (72MHz main frequency, 12-bit ADC) is selected as the main controller. 5GPIO pins are used to implement row-column addressing: PA0-PA2 control the CD4051 (8-channel

ISSN: 2414-1895 DOI: 10.6919/ICJE.202603_12(3).0047

analog multiplexer) to select 8 columns of sensors, and PA3-PA4 control the CD4052 (dual 4-channel analog multiplexer) to select 4 rows of sensors, as shown in Fig. 2. Compared with the traditional direct driving scheme (requiring 12 GPIO pins), this design reduces IO occupation by 58%, and accurately adapts to the compact layout of the 4×8 irregular array. The USART1 serial port transmits data at a baud rate of 115200 bps, combined with CRC-16 checksum to ensure no packet loss of 32-byte pressure data per frame.

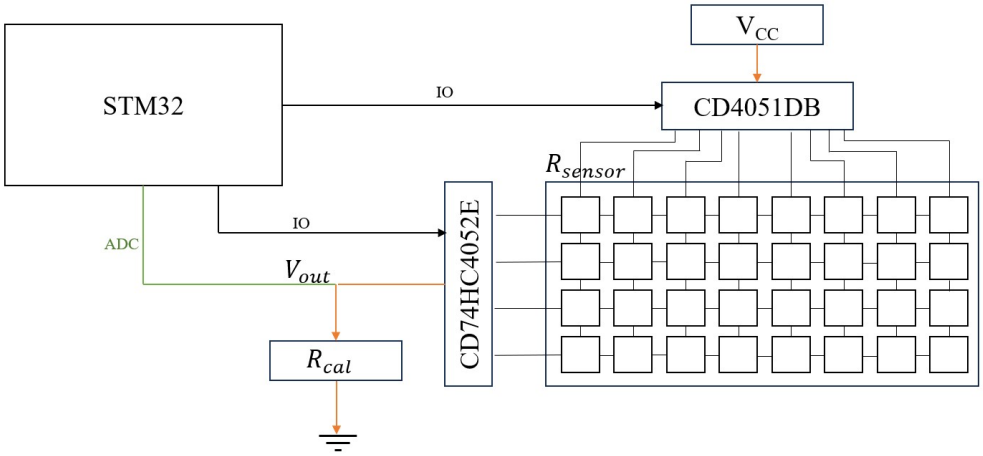

Fig. 2 System circuit diagram

Signal Conditioning Circuit:

The sensor is connected in series with a 51kΩ calibration resistor to form a voltage divider circuit (V_{CC}=3.3V). According to the voltage division formula:

$$V_{out} = \frac{R_{sensor}}{R_{sensor} + R_{cal}} \times V_{cc}(V_{cc} = 3.3V) \quad (1)$$

When the sensor resistance R_{sensor} changes in the range of 15~250 kΩ, the output voltage V_{out} corresponds to 0.73~2.75V, covering 22%~83% of the ADC full scale. This design avoids the deterioration of signal-to-noise ratio in the low resistance region and nonlinear distortion in the high resistance region. The static current of the circuit is less than 0.065mA, and the input impedance is matched with the ADC (≥50kΩ) to reduce signal attenuation error.

3.2 Conductance-Pressure Sensing Model

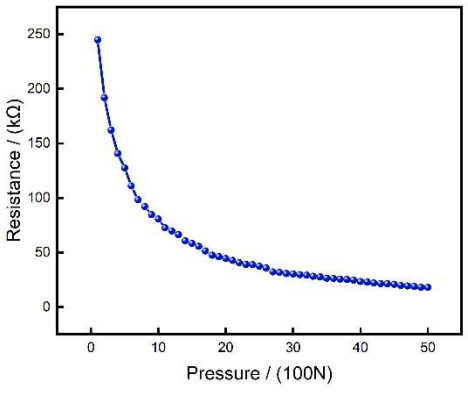

Fig. 3 Resistance-pressure diagram

ISSN: 2414-1895 DOI: 10.6919/ICJE.202603_12(3).0047

Experimental results show that the sensor resistance decreases nonlinearly with increasing pressure, from 244.87kΩ at 10g to 17.88kΩ at 5000g, as plotted in Fig. 3.

When the resistance is converted to conductance (G=1/R), the conductance exhibits a significant linear correlation with pressure, as shown in Fig. 4. The linear fitting model is expressed as:

$$G = 0.001P + 0.0023 \quad (R^2 = 0.992) \tag{2}$$

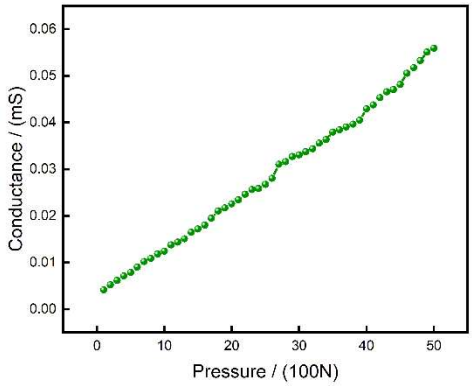

Fig. 4 Conductance-pressure diagram

The physical mechanism of this linear relationship is that the number of internal conductive paths of the sensor increases with rising pressure. Based on the linear model, the pressure inversion formula is derived as:

$$P = 1000 \times \left(\frac{1}{R} - 0.0023\right) \tag{3}$$

The measured calculation error of this formula is less than 5%, which takes into account clear physical meaning and real-time calculation efficiency, and provides a theoretical basis for dynamic pressure monitoring. The resistance is calculated from the measured output voltage by:

$$R = \frac{3.3 \times 51000}{V_{out}} - 51000 \tag{4}$$

4. Design of Data Acquisition Algorithm

4.1 Initial Full-Array Scanning and Flag Matrix Construction

After the system is started, a full-traversal scan is performed once, and 32 sensing nodes (4rows × 8columns) are selected sequentially through CD4052/CD4051. The CD4051 controls the column address (0~7) and the CD4052 controls the row address (0~3), generating 0~31 channel codes to complete node gating. After the divided signal is collected by the 12-bit ADC, the resistance value is calculated by formula (4), and then converted to the pressure value by formula (3).

To quickly screen effective pressure regions, a two-dimensional marker array flag[8][4] is defined (row index corresponds to 8 columns of sensors, column index corresponds to 4 rows of sensors). When the node pressure is less than 50g, it is marked as 0 (no pressure), and when it is ≥50g, it is marked as 1 (effective pressure). The total time of the full-traversal scan is about 65ms (including 1μs ADC sampling and 1ms calculation time), which provides a judgment basis for subsequent directional scanning.

ISSN: 2414-1895 DOI: 10.6919/ICJE.202603_12(3).0047

4.2 "1+4" Fast Scanning Optimization Strategy

The system adopts an optimized mode of "1 initial scan + 4 directional scans". The initial full-traversal scan generates a flag matrix to filter out non-pressure nodes (8~12 effective nodes are retained on average), and the subsequent 4 scans only perform four-directional redundant measurement on the effective nodes in the order of row priority, column priority, row reverse order, and column reverse order.

The core advantages of this strategy are reflected in two aspects. First, efficiency improvement: the total scanning time is reduced from 325ms of the traditional full-traversal scheme to 145ms, with a 51% efficiency improvement, which meets the requirement of 10 Hz sampling rate. Second, accuracy guarantee: the four-directional scanning covers the pressure diffusion path (such as contact sliding), reduces the dynamic miss detection rate. Combined with cross-cycle median filtering, the pressure fluctuation range is compressed from ±15g to ±5g, achieving the optimal trade-off between real-time performance and reliability.

5. Host Computer System Design

5.1 Multi-Thread Architecture and Interface Design

The host computer is developed based on Python3.9 and PyQt6. The interface includes 3 functional buttons (serial port selection, start, pause) and a QGraphicsView heatmap display control, as shown in Fig. 5. A multi-threaded architecture is adopted to decouple data communication and interface response: The SerialReader sub-thread (inherited from QThread) asynchronously reads serial port data at 115200bps through the pyserial library, and transmits the data to the main thread through the pyqtSignal slot mechanism; The main thread reshapes the received 32-dimensional string array into a 4×8 pressure matrix through numpy, and triggers the heatmap update with a QTimer (500ms period) to avoid interface jamming.

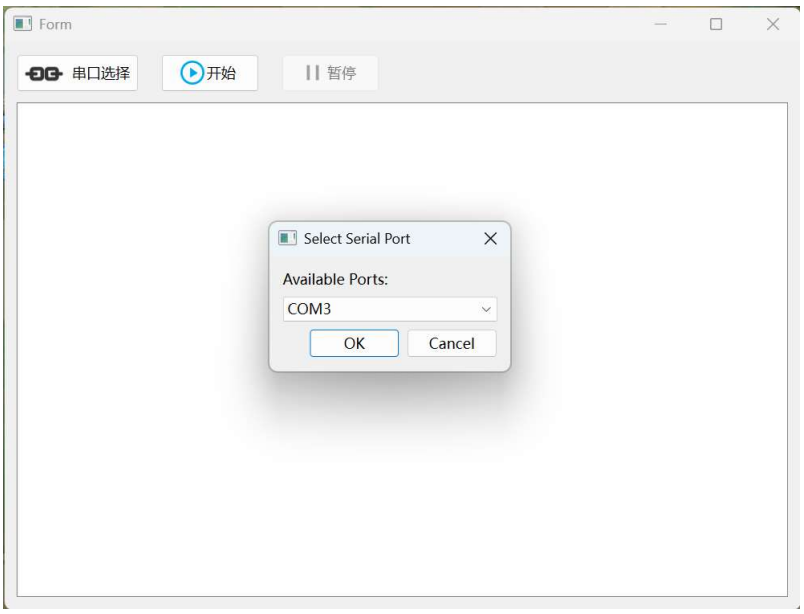

Fig. 5 Serial port selection interface of the host computer

5.2 Heatmap Visualization Optimization

The heatmap is drawn based on the seaborn library. The 32-dimensional data is converted into a 4×8 matrix through numpy.reshape to match the physical layout of the sensor. A custom four-segment gradient color scale (white→green→yellow→red) with 100 color levels is set to realize visual hierarchical mapping of pressure values, and the annot=True parameter is enabled to automatically embed numerical labels.

ISSN: 2414-1895 DOI: 10.6919/ICJE.202603_12(3).0047

This design has three advantages: first, the color scale mapping is optimized based on color psychology to reduce pressure interpretation error; second, seaborn's anti-aliasing rendering and cross-platform DPI adaptive mechanism ensure consistent display on Windows/Linux systems; third, it supports pickle data serialization, realizes historical playback and offline analysis of pressure distribution, and achieves 30fps smooth rendering on embedded hardware such as Raspberry Pi4B, meeting the real-time requirements of offline analysis.

6. System Testing and Result Analysis

6.1 Test Scheme

System tests are carried out in scenarios simulating practical applications, covering two dimensions: hardware function verification and software performance evaluation. The hardware test verifies the stability of the CD4052/CD4051 row-column gating circuit, ADC acquisition accuracy (±0.05%FSR), and voltage division consistency of the 51kΩ calibration resistor based on the STM32-driven 4×8 flexible array sensor system. The software test runs the complete data acquisition algorithm and host computer program, focusing on the evaluation of real-time performance and data integrity.

Test cases are designed to cover multi-scenario pressure detection requirements: single-point detection, where calibrated pressure of 20~25g (low pressure region) and 2000~3000g (high pressure region) is applied to the center, edge and random nodes of the sensor; multi-point detection, where 3 randomly selected nodes are simultaneously applied with 0~50g pressure, and 12 nodes (2×3 grid and two 3-grid regions) are applied with 0~1000g pressure, to verify the multi-point recognition capability and scanning synchronization of the system; and efficiency comparison, where the time consumption difference between the traditional full-traversal mode and the optimized algorithm in single-point/multi-point scenarios is compared to quantify the algorithm optimization effect. This multi-dimensional and multi-granularity test design comprehensively verifies the performance of the system in static, dynamic and complex pressure distribution scenarios.

6.2 Test Results and Performance Evaluation

The key test data are summarized in Table1.

Table 1. Critical validation test data

Test the scenario	Pressure range/(N)	Average error/(N)	Acquisition time-consuming/(ms)
Single Point (Center)	0.2~0.25	±0.006	145
Single Point (Edge)	20~30	±0.2	145
Multipoint (3 points)	0.2~0.4	±0.05	152
Multi-point (12 nodes)	0~10	±0.50	158

The test results show that the system meets the design requirements in terms of accuracy, efficiency and visualization. In terms of accuracy, the measurement error in the single-point low pressure region (0.20~0.25N) is stable within ±0.6N, as shown in Fig. 6a; in the high pressure region (20~30N), the error increases to ±0.20N due to the nonlinear characteristics of the sensor, and interference data (3.4N) appears above the test point (24N) caused by the thin film process and data crosstalk, as shown in Fig. 6b; the measurement error of 3-point pressure is within ±5N, as shown in Fig. 6c; in multi-point detection, the error increases with the number of nodes (±0.50N for 12 nodes) due to the adjacent pressure coupling effect, and one node has missing readings, but it still meets the design threshold of ±100g, as shown in Fig. 6d.

ISSN: 2414-1895 DOI: 10.6919/ICJE.202603_12(3).0047

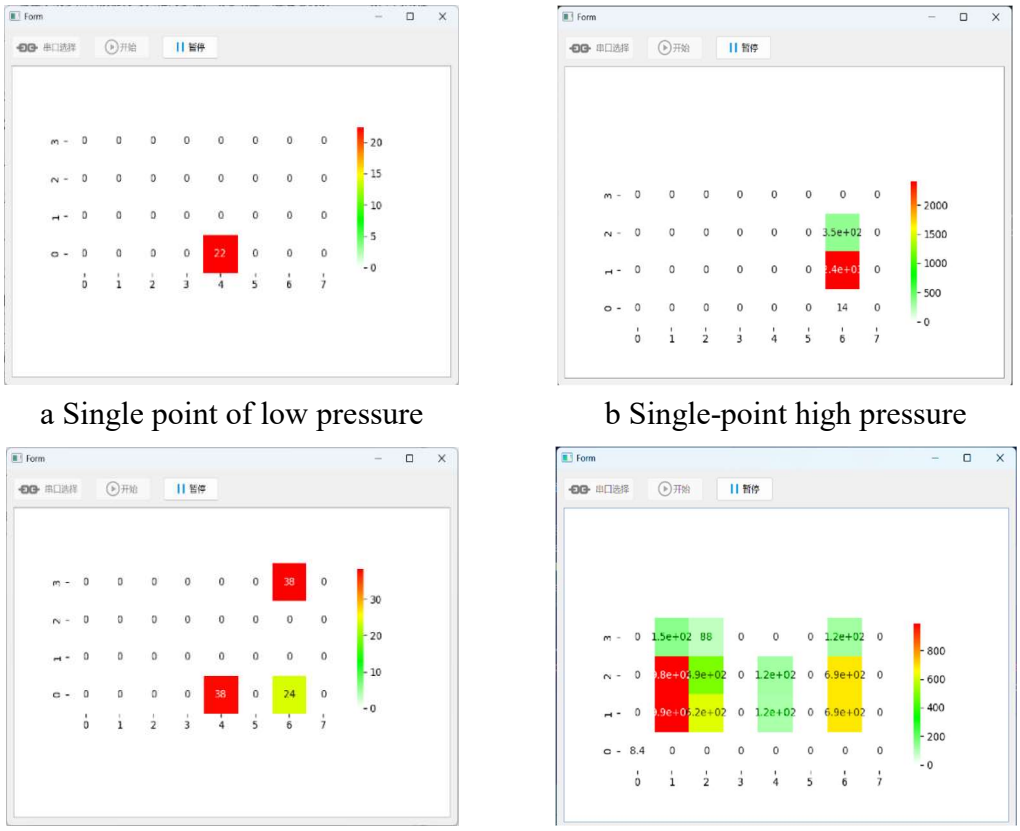

a Single point of low pressure b Single-point high pressure

c 3 points of pressure d 12 points of pressure

Fig. 6 Single-point and multi-point stress testing and display

In terms of efficiency, the time consumption of the optimized "1+4" algorithm only increases by about 5% in the multi-point detection scenario (145ms for single point → 158ms for 12 points), which is 51% higher than the traditional full-traversal scheme (325ms). In the dynamic pressure test, the system response latency is less than 50ms, and the standard deviation of pressure fluctuation is ±50N, which meets the real-time requirements. The above results verify the high accuracy, high efficiency and strong robustness of the system in complex scenarios, and provide a reliable guarantee for the practical application of flexible array sensors.

6.3 Optimization Directions

Based on the test results, the system can be further optimized in the following aspects. For accuracy improvement, the hardware design of the ADC circuit can be optimized, and a higher resolution ADC chip can be used to reduce the error in the analog-to-digital signal conversion. Meanwhile, more in-depth experiments on the relationship between pressure and resistance can be carried out, more influencing factors can be considered, and the pressure inversion formula can be further optimized to improve measurement accuracy. For speed optimization, the data acquisition algorithm can be further refined to reduce unnecessary calculation and data transmission overhead, such as improving the two-dimensional array scanning algorithm to reduce the number of scans or optimize the scanning path. In addition, the serial communication protocol can be optimized to improve the efficiency of data transmission, so as to further enhance the overall performance of the system to better meet practical application requirements.

7. Summary

In this study, an efficient data acquisition system for a 4×8 irregular flexible array sensor is constructed based on the STM32 main control chip and CD4052/CD4051 analog multiplexers. At the hardware level, the system realizes wide-range pressure sensing (0~5000g) and low-noise signal

ISSN: 2414-1895 DOI: 10.6919/ICJE.202603_12(3).0047

conditioning with a voltage error of ±0.02V. At the algorithm level, the proposed "1+4" fast scanning strategy reduces single-frame scanning time from 325ms to 145ms with a 51% efficiency improvement, and achieves a measurement accuracy of ±0.5N through the established linear conductance-pressure model. The host computer system developed with a Qt multi-threaded architecture and Seaborn heatmap module realizes dynamic data visualization and serialized storage of pressure distribution.

Experiments verify the practicability of the system in medical and industrial application scenarios with an end-to-end latency of ≤50ms. This work provides a scalable technical path for the low-cost and high-real-time application of non-standard array sensors, and fills the technical gap in low-cost real-time monitoring for irregular flexible pressure sensor arrays. In future work, the dynamic path planning algorithm can be further optimized and extended to larger-scale sensor arrays, so as to improve the adaptability of the system in more complex application scenarios.

Acknowledgments

Guangdong provincial fund for development strategy of Science and Technology Innovation (No.2024090505, No.2025020304).

References

[1] Chen Y, Zheng L, Yin W, et al. Flexible Sensor-based Whole-body Biomechanics of Exoskeleton-assisted Patient Handling[J]. Proceedings of the Human Factors and Ergonomics Society Annual Meeting, 2024, 68(1): 651-654.

[2] Godoy C J A, Pérez G I. Integration of Sensor and Actuator Networks and the SCADA System to Promote the Migration of the Legacy Flexible Manufacturing System towards the Industry 4.0 Concept[J]. Journal of Sensor and Actuator Networks, 2018, 7(2): 23.

[3] Ma Y, Du K, Zhou D, et al. Automatic precision robot assembly system with microscopic vision and force sensor[J]. International Journal of Advanced Robotic Systems, 2019, 16(3): 1729881419851619.

[4] Zhang X, Wang Y, Zhang L, et al. Facile preparation of porous MXene/cellulose nanofiber composite for highly-sensitive flexible piezoresistive sensors in e-skin[J]. Chemical Engineering Journal, 2025, 505: 159369.

[5] Mei J, Brunton L S, Kutz N J. Mobile Sensor Path Planning for Kalman Filter Spatiotemporal Estimation[J]. Sensors (Basel, Switzerland), 2024, 24(12): 3727.

[6] Huang L, Chen Z, Yang Z, et al. Advancing Healthcare Accessibility: Fusing Artificial Intelligence with Flexible Sensing to Forge Digital Health Innovations[J]. BME Frontiers, 2024: 50062.

[7] Bing L, Hong W. PAPR reduction and low power-consumption LDO in OFDM transceiver[J]. Analog Integrated Circuits and Signal Processing, 2025, 122(3): 34.

[8] Zhang H X, Wang B, Zhou B, et al. Recent advances in MXene-based flexible pressure sensors for medical monitoring[J]. Rare Metals, 2025: 1-33.